Three-Dimensional Neutronics Analysis for the ITER Divertor Cassette

M.E. Sawan

November 1997

UWFDM-1056

FUSION TECHNOLOGY INSTITUTE

UNIVERSITY OF WISCONSIN

MADISON WISCONSIN

ITER/US/97-IV-DV-10

Three-Dimensional Neutronics Analysis for the ITER Diagnostic Cassette

Mohamed E. Sawan

Fusion Technology Institute
University of Wisconsin-Madison
1500 Engineering Drive
Madison, WI 53706

November 1997

UWFDM-1056

DISCLAIMER

This report is an account of work undertaken within the framework of the ITER EDA Agreement. Neither the ITER Director, the Parties to the ITER Agreement, the U.S. DOE, the U.S. Home Team Leader, the U.S. Home Team, the IAEA or any agency thereof, or any of their employees, makes any warranty, express or implied, or assumes any legal liability or responsibility for the accuracy, completeness, or usefulness of any information, apparatus, product, or process disclosed, or represents that its use would not infringe privately owned rights. Reference herein to any specific commercial product, process, or service by trade name, trademark, manufacturer, or otherwise, does not necessarily constitute or imply its endorsement, recommendation, or favoring by the parties to the ITER EDA Agreement, the IAEA or any agency thereof.

The views and opinions of authors expressed herein do not necessarily state or reflect those of the ITER Director, the Parties to the ITER Agreement, the U.S. DOE, the U.S. Home Team Leader, the U.S. Home Team, the IAEA or any agency thereof.

Abstract

3-D neutronics and shielding analyses have been performed for the divertor region. A detailed 3-D model has been developed for the divertor region of the ITER Detailed Design. Each divertor cassette in the model was divided into 103 regions to provide detailed spatial distribution of nuclear heating and radiation damage. The layered configurations of the dome PFC and vertical targets were modeled accurately with the front tungsten layer modeled separately. Separate regions are included in the model to represent the mechanical attachments and coolant pipe connections for the dome, vertical targets, and wings. The neutronics calculations have been performed using the continuos energy MCNP-4A code with cross section data from FENDL-1 to determine the detailed spatial distribution of the nuclear parameters in the divertor cassette. The nuclear parameters were provided at the 103 cassette regions used in the model. These parameters included power density, atomic displacement and helium production. The largest heating and damage occurs in the dome PFC which has full view of the plasma. The power density in the W PFC at the dome is 16.4 W/cm^3. The total nuclear heating in the 60 divertor cassettes is 101.6 MW with the major contributors being the dome, vertical targets, and wings. The peak helium production in the vacuum vessel behind the pumping ducts is 0.2 He appm/FPY implying that rewelding is feasible. In addition, helium production in the divertor port wall is less than 0.04 He appm/FPY.

1. INTRODUCTION

The divertor cassette design went through several changes to improve its performance. Neutronics and shielding features were considered for the design variations. The latest ITER design is the Detailed Design [1]. The design utilizes 60 divertor cassettes with vertical targets and a central dome. Knowledge of nuclear heating and radiation damage levels in the different components of the divertor cassette is essential for proper design analysis. 20 large divertor ports are utilized for assembly and disassembly of the divertor cassettes and for vacuum pumping. Radiation damage to parts of the vacuum vessel (VV) in the divertor region need to be quantified to assess the feasibility of rewelding. Due to the geometrical complexity of the divertor region, three-dimensional (3-D) analyses are required. This design was preceded by the Interim Design of ITER [2]. Three-dimensional neutronics and shielding calculations were performed for the divertor region in the Interim Design to determine the nuclear parameters in the divertor cassette and surrounding vacuum vessel and TF coils [3]. Several changes in both geometrical configuration and material composition have been employed recently in the divertor cassette design. In addition, more detailed spatial distribution of nuclear parameters in the cassette was needed for precise mechanical and thermal-hydraulics design. A detailed 3-D model has been developed for the divertor cassette in the ITER Detailed Design to incorporate the design changes and determine more detailed nuclear parameter profiles.

2. THREE-DIMENSIONAL CALCULATIONAL MODEL

Due to the geometrical complexity of the divertor region, 3-D models are required to properly determine the nuclear parameters. 3-D neutron-gamma transport calculations have been performed for the divertor region. The continuous energy, coupled neutron-gamma-ray Monte Carlo code MCNP-4A [4] has been used. The nuclear data used is based on the FENDL-1 evaluation [5]. The detailed geometrical configuration of the divertor cassette has been modeled for 3-D neutronics calculations. The drawings provided by the Joint Central Team (JCT) at Garching for the Detailed ITER Design are the basis for the 3-D modeling. The model represents a nine degree toroidal sector of ITER. Hence, it includes one and a half cassettes with the associated nominal 1 cm gaps between adjacent cassettes. The model includes in detail the high heat flux plasma facing components (PFC), the vertical targets, the wings with associated plates, and the gas boxes, as well as the central dome and cassette

bodies. The 37.5 cm wide and 17.5 cm thick divertor pumping duct at the bottom of each cassette is included in the model. The rails upon which the cassettes move toroidally during maintenance are also included. Each divertor cassette in the model was divided into 103 regions to provide detailed spatial distribution of nuclear heating and radiation damage. The layered configurations of the dome PFC and vertical targets were modeled accurately with the front tungsten layer modeled separately. Separate regions are included in the model to represent the mechanical attachments and coolant pipe connections for the dome, vertical targets, and wings. Fig. 1 shows a vertical cross section of the cassette model at a toroidal location at the center of the cassette through the pumping ducts. Figures 2, 3 and 4 give the numbers used to identify the cells used in the MCNP calculations for determining the spatial distribution of the nuclear parameters.

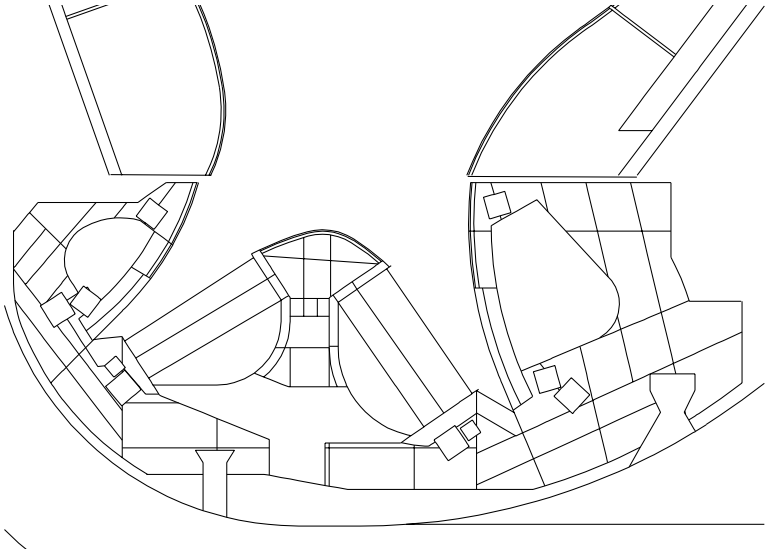

Fig. 1. Vertical cross section at the middle of the cassette model.

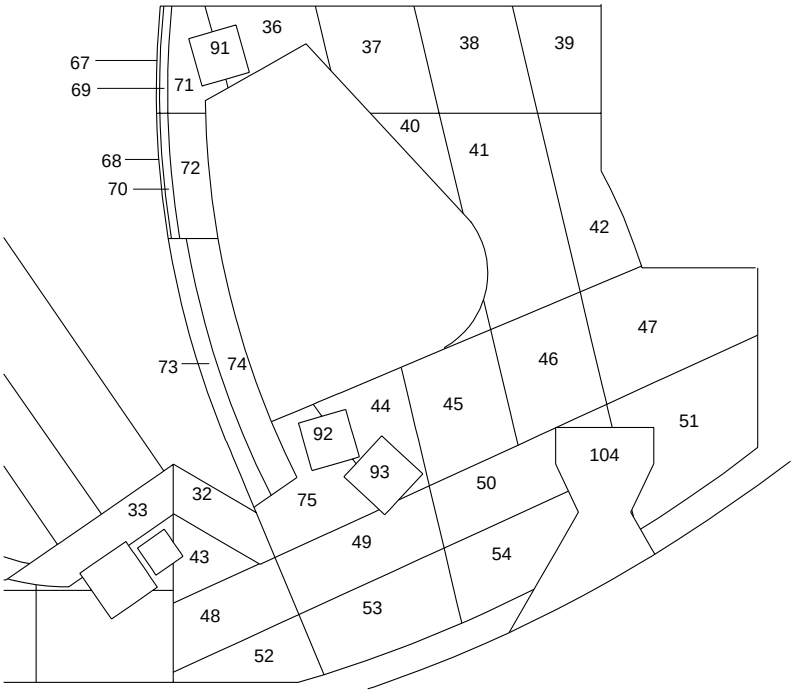

Fig. 2. Vertical cross section in the outer part of cassette showing the cells used to determine the spatial variation of nuclear parameters.

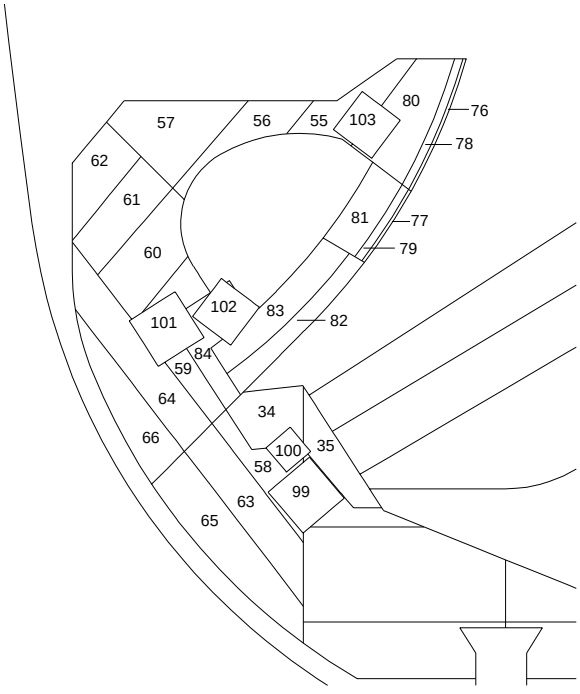

Fig. 3. Vertical cross section in the inner part of cassette showing the cells used to determine the spatial variation of nuclear parameters.

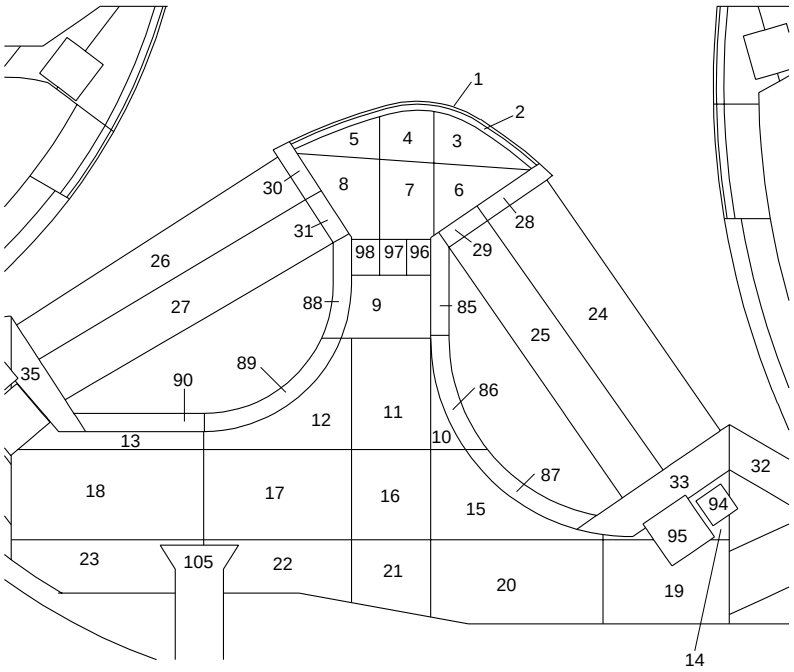

Fig. 4. Vertical cross section in the central part of cassette showing the cells used to determine the spatial variation of nuclear parameters.

The divertor cassette model has been integrated with the general ITER model based on the Interim ITER Design. The integrated model includes detailed modeling of the first wall, blanket with associated coolant manifolds and back plates, VV, TF coils, central solenoid, and PF coils. While Be is used as the plasma facing material at the first walls of the blanket modules, tungsten is used for the inboard and outboard baffle modules above the divertor cassette. All toroidal and poloidal gaps between adjacent blanket modules are included. The major vacuum vessel penetrations are included in the model. This includes the divertor port at the bottom of the reactor. Due to symmetry, only 1/40 of the reactor is modeled with surrounding reflecting boundaries. The model includes half a TF coil and half a divertor port. The divertor port is 254.5 cm high with a width increasing from 97 cm at the bottom to 176 cm at the top. The port wall is 20 cm thick and is assumed to consist of 80% 316SS and 20% water. No additional shielding is included around the port. The blanket design in the ITER Interim Design was used since the blanket design was not fully developed in the Detailed Design. Since most of the design changes in the blanket are expected to be in the back plate, module attachment and manifolds, the impact will be mainly on shielding and streaming through the large ports and the impact on nuclear parameters in the divertor cassette will be minimal.

The output of the MCNP geometry plotting routine given in Fig. 5 shows a vertical cross section through the middle of the vacuum vessel ports. The detailed reactor geometrical modeling is illustrated. Figure 6 is a horizontal cross section at z= -6 m in the middle of the divertor port. The divertor pumping ducts in the divertor cassettes are shown in this figure. Also shown is the part of the TF coil adjacent to the divertor port. A coil case which is about 20 cm thick surrounds the winding pack. Several splitting surfaces have been added in the divertor region to allow for utilizing the geometry splitting with Russian Roulette variance reduction techniques employed in MCNP, needed to improve the accuracy of the calculated nuclear responses.

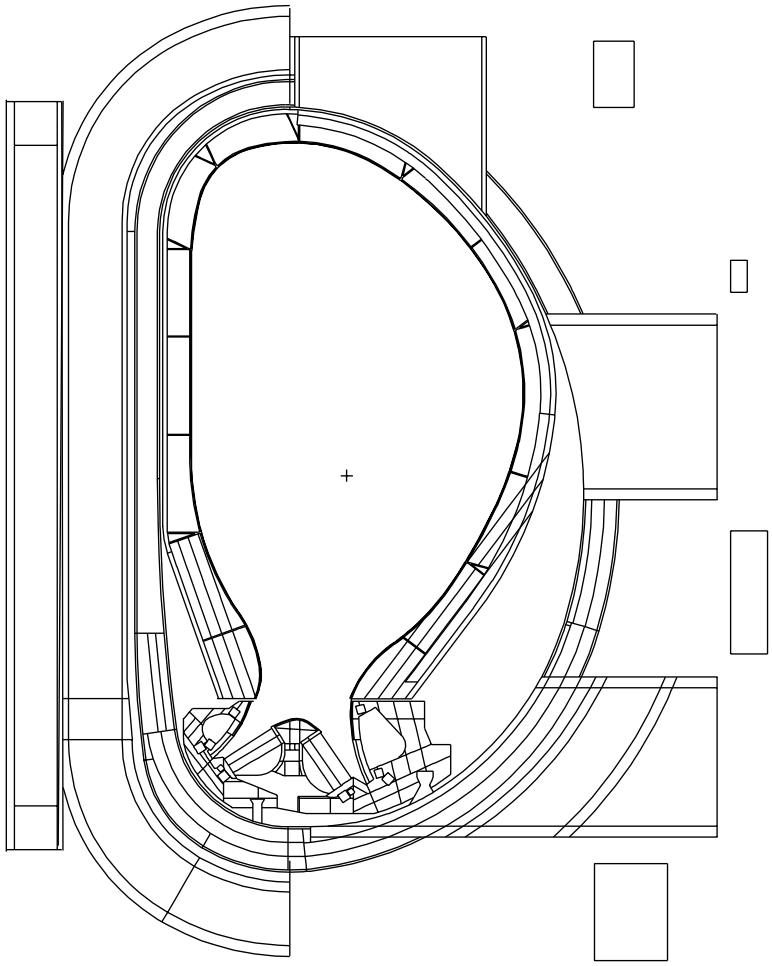

Fig. 5. Vertical cross section through the VV ports of the ITER 3-D model for MCNP calculations.

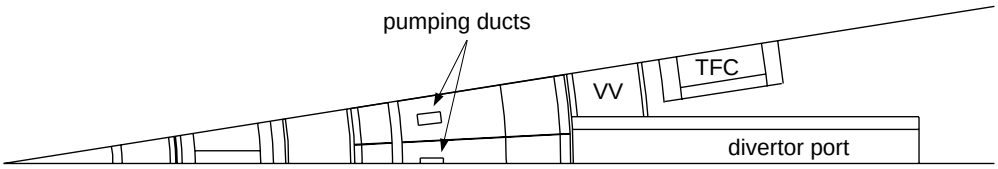

Fig. 6. Horizontal cross section of the 3-D model at z= -6 m.

A combination of cones, tori, cylinders, and planes was utilized for accurate modeling of the geometry. A total of 543 surfaces has been used in the model, of which 175 are fourth degree tori. The model employs 593 geometrical cells. The volumes of the different cells and the areas of surfaces of interest have been determined stochastically by ray tracing. In this calculation, all cells are assumed to not include any material and the geometrical model has been sprayed by 20 million particles at random directions. This calculation serves also as a means for geometry checking by making sure that each point in space belongs to one of the cells used in the model. This calculation provided a successful check for the geometrical model.

A source subroutine has been written to modify MCNP to sample source neutrons from the source distribution in the ITER plasma provided numerically by the San Diego JCT at 1600 mesh points. Cell flux and energy deposition tallies are used to determine the volume averaged parameters and total nuclear heating in the components of the divertor. The appropriate material compositions are used for the different cells of the model. The VV consists of two 4 cm thick 316SS plates sandwiching a shielding region made of 60% 316SS and 40% water. The winding pack of the TF coil consists of 43.2% SS, 11.7% Cu, 2.9% Nb_3Sn, 7.4% bronze, 16.8% liquid He, and 18% insulator (epoxy with 70% R-glass). The material composition used for the divertor cassette is given in Table 1. The calculation has been performed using 50,000 source particles yielding statistical uncertainties of less than 5% in the calculated nuclear responses at the locations of interest. The calculation used 20 hours of CPU on the Cray-2. The results are normalized to the nominal fusion power of 1500 MW. The end of life fluence related radiation effects have been determined for 1 full power year (FPY) of operation corresponding to a fluence of 1 $MW \cdot a/m^2$.

Table 1. Material Composition

Dome PFC	1 cm W 2 cm 75% Cu, 25% water Cu dome body 85% Cu, 15% water SS dome body 75% SS, 25% water
Wings	16% W, 79% Cu, 5% water packing fraction: 21% outer, 26% inner
Gas Box Liners and Wing Plates	8% W, 74% Cu, 18% water
Vertical Targets	top section: 1 cm W 2.5 cm 82% Cu, 18% water back region 97% SS, 3% water lower section: 5.5 cm 89% C, 4% Cu, 7% water back region 97% SS, 3% water
Cassette Body	80% SS, 20% water
Mechanical Attachments	100% SS
Coolant Pipe Connections	70% SS, 30% water
Rails	100% SS

4. NUCLEAR PARAMETERS IN THE DIVERTOR CASSETTE

The neutronics parameters have been calculated in the different components of the divertor cassette. These parameters included nuclear heating, atomic displacement and helium production. The radiation damage was calculated for the structural material used in each region. The volume averaged parameters were determined for 103 segments of the cassette using cell flux and energy deposition tallies. These results are given in Table 2. The zone numbers correspond to the numbers given in Figs. 2-4. The largest heating and damage occurs in the dome PFC which has a full view of the plasma and has the largest neutron wall loading. The power density in the W PFC at the dome is 16.4 W/cm^3. The W PFC at the top of the vertical targets experience relatively high levels of heating and damage. The rest of the vertical targets and wings experience moderate levels of heating and damage with values dropping rapidly as one moves deeper in the cassette body. In general, the nuclear parameters in the inboard side of the cassette are lower than in the outboard side that has a larger view of the plasma. Atomic displacements in Cu are slightly higher than in SS (by ~10% at the front and ~30% at the back) while helium production is much lower (about two-thirds at the front and an order of magnitude lower at the back) because of the higher threshold energy of nuclear reactions producing helium. The nuclear heating map in the cassette is given in Fig. 7 based on the 3-D results. Table 3 gives the total amount of nuclear heating for each of the zones used in the MCNP calculation. The total nuclear heating has been calculated for the 60 divertor cassettes to be 101.6 MW. The major contributors are the dome, vertical targets, and wings.

Table 2. Spatial Distribution of Nuclear Responses in the Divertor Cassette

Zone Number	Power Density (W/cm^3)	dpa in Structure (dpa/FPY)	He Prod. in Structure (appm/FPY)
Dome PFC			
1	1.64512E+01	1.26505E+00 W	7.27511E-01 W
2	5.43031E+00	3.50658E+00 Cu	3.14168E+01 Cu
Dome Body			
3	3.44687E+00	1.63951E+00 Cu	1.14537E+01 Cu
4	3.23213E+00	1.46601E+00 Cu	1.04745E+01 Cu
5	3.96214E+00	2.15013E+00 Cu	1.68394E+01 Cu
6	1.21992E+00	3.63048E-01 SS	1.01488E+01 SS
7	6.02719E-01	1.42000E-01 SS	4.64688E+00 SS
8	1.22387E+00	3.96199E-01 SS	1.03569E+01 SS
9	2.29696E-01	4.00311E-02 SS	1.53968E+00 SS
Central Body			
10	3.63142E-01	9.74313E-02 SS	2.53758E+00 SS
11	1.52880E-01	2.52851E-02 SS	1.06495E+00 SS
12	2.37689E-01	5.98621E-02 SS	1.74341E+00 SS
13	2.92007E-01	9.37217E-02 SS	2.27798E+00 SS
14	2.91206E-01	1.07046E-01 SS	2.14466E+00 SS
15	2.84445E-01	8.49762E-02 SS	2.13524E+00 SS
16	6.94011E-02	1.12960E-02 SS	4.92276E-01 SS
17	1.00319E-01	2.32558E-02 SS	7.45732E-01 SS
18	9.29792E-02	2.48528E-02 SS	7.13030E-01 SS
19	4.10597E-02	1.00562E-02 SS	2.89277E-01 SS
20	8.05709E-02	2.13133E-02 SS	6.12298E-01 SS
21	2.71199E-02	4.45065E-03 SS	1.91279E-01 SS
22	2.44052E-02	4.26435E-03 SS	1.66953E-01 SS
23	5.52325E-03	1.21668E-03 SS	3.60974E-02 SS
Wings			
24	3.07969E+00	1.74438E+00 Cu	1.42428E+01 Cu
25	1.07809E+00	6.47604E-01 Cu	3.50816E+00 Cu
26	2.98566E+00	1.62231E+00 Cu	1.38155E+01 Cu
27	1.27749E+00	6.80000E-01 Cu	4.40209E+00 Cu
Wing Plates			
28	2.80129E+00	1.18408E+00 Cu	8.63663E+00 Cu
29	8.48758E-01	1.96071E-01 Cu	6.23878E-01 Cu
30	3.08058E+00	1.41322E+00 Cu	1.19228E+01 Cu
31	7.66809E-01	2.41882E-01 Cu	8.12182E-01 Cu
32	1.51048E+00	6.43523E-01 Cu	5.13236E+00 Cu
33	1.09830E+00	4.88210E-01 Cu	3.55298E+00 Cu
34	8.87191E-01	2.44223E-01 Cu	1.10380E+00 Cu
35	7.09406E-01	2.81615E-01 Cu	1.86362E+00 Cu

Table 2. Spatial Distribution of Nuclear Responses in the Divertor Cassette
(Continued)

Zone Number	Power Density (W/cm^3)	dpa in Structure (dpa/FPY)	He Prod. in Structure (appm/FPY)
Outer Leg			
36	5.07270E-01	1.12983E-01 SS	3.66545E+00 SS
37	1.48334E-01	2.27054E-02 SS	1.06637E+00 SS
38	1.44480E-02	1.88313E-03 SS	8.63420E-02 SS
39	4.68094E-03	1.07628E-03 SS	3.60617E-02 SS
40	2.67502E-01	5.01538E-02 SS	2.06120E+00 SS
41	1.05625E-01	1.55813E-02 SS	7.56098E-01 SS
42	5.69996E-03	7.54240E-04 SS	3.40215E-02 SS
43	2.93069E-01	9.43302E-02 SS	2.11672E+00 SS
44	1.44584E-01	2.25009E-02 SS	1.11943E+00 SS
45	8.04193E-02	1.09916E-02 SS	5.93138E-01 SS
46	2.03556E-02	2.41850E-03 SS	1.31798E-01 SS
47	2.33981E-03	4.76464E-04 SS	1.64483E-02 SS
48	5.21032E-02	1.32551E-02 SS	3.62345E-01 SS
49	3.31166E-02	7.59347E-03 SS	2.50403E-01 SS
50	9.09418E-04	9.10893E-05 SS	5.15067E-03 SS
51	8.14602E-04	1.44283E-04 SS	5.98673E-03 SS
52	6.08651E-03	1.18973E-03 SS	3.99173E-02 SS
53	3.43677E-03	5.08195E-04 SS	2.09634E-02 SS
54	1.52522E-04	1.62949E-05 SS	1.13074E-03 SS
Inner Leg			
55	2.75638E-01	4.35025E-02 SS	1.99259E+00 SS
56	1.87814E-01	2.81319E-02 SS	1.41326E+00 SS
57	7.06411E-02	8.39373E-03 SS	5.12446E-01 SS
58	1.20278E-01	3.18610E-02 SS	8.62570E-01 SS
59	1.23636E-01	2.03488E-02 SS	9.23703E-01 SS
60	8.58328E-02	1.20511E-02 SS	6.37679E-01 SS
61	3.49502E-02	3.09739E-03 SS	2.28392E-01 SS
62	1.56698E-02	1.55726E-03 SS	1.03757E-01 SS
63	3.11789E-02	6.58251E-03 SS	2.09019E-01 SS
64	2.01229E-02	3.15133E-03 SS	1.32061E-01 SS
65	5.73569E-03	1.10182E-03 SS	3.72236E-02 SS
66	6.69695E-03	1.14459E-03 SS	4.16772E-02 SS

Table 2. Spatial Distribution of Nuclear Responses in the Divertor Cassette
(Continued)

Zone Number	Power Density (W/cm^3)	dpa in Structure (dpa/FPY)	He Prod. in Structure (appm/FPY)
Outer Vertical Target			
67	1.18348E+01	8.71309E-01 W	4.79312E-01 W
68	9.18024E+00	6.50661E-01 W	2.95431E-01 W
69	3.08390E+00	1.93672E+00 Cu	1.32544E+01 Cu
70	2.19196E+00	1.33188E+00 Cu	7.67015E+00 Cu
71	1.40946E+00	7.88720E-01 SS	8.78725E+00 SS
72	8.63541E-01	4.31594E-01 SS	4.64435E+00 SS
73	8.02462E-01	9.97240E-01 Cu	6.89184E+00 Cu
74	7.64140E-01	2.61362E-01 SS	4.01073E+00 SS
75	2.18959E-01	8.04580E-02 SS	1.02179E+00 SS
Inner Vertical Target			
76	8.41348E+00	3.50574E-01 W	7.49133E-02 W
77	5.78643E+00	2.75823E-01 W	1.72104E-02 W
78	1.82793E+00	7.79391E-01 Cu	1.88168E+00 Cu
79	1.24546E+00	5.85931E-01 Cu	1.06106E+00 Cu
80	6.86241E-01	2.76053E-01 SS	3.08816E+00 SS
81	5.07397E-01	2.00960E-01 SS	2.09148E+00 SS
82	3.73224E-01	3.37171E-01 Cu	7.91757E-01 Cu
83	5.16947E-01	1.12597E-01 SS	2.63015E+00 SS
84	2.39251E-01	4.54780E-02 SS	1.03810E+00 SS
Gas Box Liner			
85	6.23528E-01	1.71595E-01 Cu	3.77898E-01 Cu
86	7.78410E-01	2.50645E-01 Cu	8.40177E-01 Cu
87	7.70658E-01	2.99092E-01 Cu	1.60511E+00 Cu
88	6.17229E-01	1.57848E-01 Cu	3.08051E-01 Cu
89	6.73409E-01	2.36376E-01 Cu	1.05790E+00 Cu
90	6.96115E-01	2.67456E-01 Cu	1.56723E+00 Cu

Table 2. Spatial Distribution of Nuclear Responses in the Divertor Cassette
(Continued)

Zone Number	Power Density (W/cm^3)	dpa in Structure (dpa/FPY)	He Prod. in Structure (appm/FPY)
Attachments and Coolant Pipe Connections			
Outer Vertical Target			
91	5.13994E-01	2.74986E-01 SS	2.16942E+00 SS
92	1.03146E-01	3.88875E-02 SS	4.38541E-01 SS
93	3.76789E-02	3.54282E-03 SS	3.05103E-01 SS
Outer Wings			
94	3.09352E-01	1.06760E-01 SS	1.41016E+00 SS
95	1.88406E-01	4.71606E-02 SS	1.57611E+00 SS
Dome			
96	2.54147E-01	4.61917E-02 SS	2.23833E+00 SS
97	1.64935E-01	2.90514E-02 SS	6.32968E-01 SS
98	2.38428E-01	4.96208E-02 SS	2.06721E+00 SS
Inner Wings			
99	1.44461E-01	3.67613E-02 SS	1.24009E+00 SS
100	2.52233E-01	1.21323E-01 SS	1.53895E+00 SS
Inner Vertical Target			
101	5.03818E-02	7.01985E-03 SS	4.58350E-01 SS
102	1.31408E-01	4.07069E-02 SS	5.76772E-01 SS
103	2.26011E-01	8.93834E-02 SS	8.39338E-01 SS
Rails			
104	1.11680E-04	2.61276E-05 SS	3.53264E-04 SS
105	6.71779E-03	2.14094E-03 SS	2.60569E-02 SS

Table 3. Total Nuclear Heating in the 60 Divertor Cassettes

Zone Number	Total Nuclear Heating in 60 Cassettes (MW)
Dome PFC	
1	6.8140
2	4.3932
Total	11.2072
Dome Body	
3	5.4197
4	4.1307
5	3.9977
6	2.1834
7	1.2322
8	2.6081
9	0.5632
Total	20.1350
Central Body	
10	0.1814
11	0.5981
12	0.6319
13	0.3591
14	0.1806
15	0.8895
16	0.1800
17	0.4906
18	0.6662
19	0.2175
20	0.5812
21	0.0574
22	0.0710
23	0.0184
Total	5.1229
Wings	
24	7.3560
25	2.1083
26	4.8105
27	2.2643
Total	16.5391
Wing Plates	
28	1.9755
29	0.3616
30	1.5014
31	0.3551
32	3.3823
33	3.2777
34	1.0875
35	0.8322
Total	12.7733

Table 3. Total Nuclear Heating in the 60 Divertor Cassettes
(Continued)

Zone Number	Total Nuclear Heating in 60 Cassettes (MW)
Outer Leg	
36	1.2752
37	0.7584
38	0.0790
39	0.0203
40	0.5583
41	1.0123
42	0.0304
43	0.5351
44	0.4136
45	0.4963
46	0.1240
47	0.0217
48	0.2017
49	0.1740
50	0.0044
51	0.0071
52	0.0171
53	0.0191
54	0.0007
Total	5.7487
Inner Leg	
55	0.2993
56	0.2282
57	0.1624
58	0.0959
59	0.1228
60	0.1582
61	0.0538
62	0.0199
63	0.0711
64	0.0515
65	0.0172
66	0.0119
Total	1.2922

Table 3. Total Nuclear Heating in the 60 Divertor Cassettes (Continued)

Zone Number	Total Nuclear Heating in 60 Cassettes (MW)
Outer Vertical Target	
67	1.9458
68	1.7764
69	1.2897
70	1.0854
71	2.4640
72	1.9748
73	1.9152
74	3.0329
75	0.8739
Total	16.3581
Inner Vertical Target	
76	1.4627
77	0.5678
78	0.7852
79	0.3063
80	1.3487
81	0.5878
82	0.4584
83	0.8573
84	0.1517
Total	6.5259
Gas Box Liner	
85	0.5639
86	0.7744
87	0.7167
88	0.5211
89	0.7520
90	0.4872
Total	3.8153

Table 3. Total Nuclear Heating in the 60 Divertor Cassettes
(Continued)

Zone Number	Total Nuclear Heating in 60 Cassettes (MW)
Attachments and Coolant Pipe Connections	
Outer Vertical Target	
91	0.5799
92	0.1289
93	0.0633
Outer Wings	
94	0.1562
95	0.2701
Dome	
96	0.1062
97	0.0756
98	0.1088
Inner Wings	
99	0.1538
100	0.0921
Inner Vertical Target	
101	0.0509
102	0.1039
103	0.1839
Total	2.0736
TOTAL IN 60 CASSETTES	**101.5913**

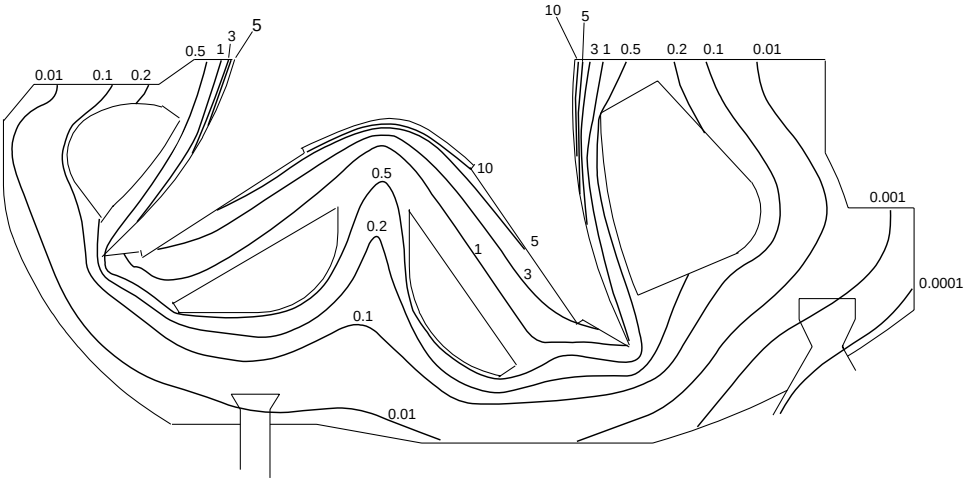

Fig. 7. Nuclear heating (W/cm^3) map in the divertor cassette.

4. NUCLEAR PARAMETERS IN VACUUM VESSEL

Streaming through the pumping ducts in the bottom of the cassette can result in damage hot spots in the VV behind it. The impact of neutron streaming through the ducts was analyzed for previous designs and recommendations regarding their configuration and size were made to minimize nuclear heating and helium production in parts of the VV behind them. In the design considered here, the pumping ducts are inclined towards the outer and inner divertor legs such that the VV behind them does not see any direct neutrons from the plasma. This helps cut down the He production which is critical for rewelding. Only low energy secondary neutrons stream through the pumping ducts. The VV results were determined both for toroidal locations away from the ducts and behind the ducts by segmenting the front surface of the VV below the cassette. The results are given in Table 4. A peaking factor of about 2 results from streaming through the ducts. The peak helium production value of about 0.2 He appm/FPY indicates that rewelding of parts of the VV behind the pumping ducts might be feasible. Since these areas of relatively high helium production are very small, the design of the VV can locate the welds away from streaming path if these values are of concern for rewelding. Another area of concern for rewelding is the divertor port where relatively high damage is expected due to neutron streaming. The helium production was calculated along the divertor port. The largest damage occurs at the location where the port wall joins to the front VV wall and drops as one moves along the port away from the plasma chamber. The peak helium production is 0.036 appm/FPY and drops to 0.005 appm/FPY at locations adjacent to the back of the TF coil. It is clear from these results that rewelding of the divertor port is feasible.

Table 4. Peak Nuclear Responses in the VV behind the Divertor Cassette

	Power Density (W/cm^3)	dpa (dpa/FPY)	He Production (appm/FPY)
Behind pumping duct	0.027	0.008	0.183
Behind cassette body	0.018	0.003	0.100

5. SUMMARY AND CONCLUSIONS

3-D neutronics and shielding analyses have been performed for the divertor region. A detailed 3-D model has been developed for the divertor region of the ITER Detailed Design. The model includes in detail the PFC, the vertical targets, the wings with associated plates, and the gas boxes, as well as the central dome and cassette bodies. Each divertor cassette in

the model was divided into 103 regions to provide detailed spatial distribution of nuclear heating and radiation damage. The layered configurations of the dome PFC and vertical targets were modeled accurately with the front tungsten layer modeled separately. Separate regions are included in the model to represent the mechanical attachments and coolant pipe connections for the dome, vertical targets, and wings. The divertor cassette model was integrated with the general ITER model that includes detailed modeling of FW, blanket with coolant manifolds and back plates, VV, TF coils, central solenoid, and PF coils based on the Interim ITER Design. Since the blanket design was not fully developed, additional changes in the general model will be included in the future. Since most of the design changes in the blanket are expected to be in the back plate, module attachment and manifolds, the impact will be mainly on shielding and streaming through the large ports and the impact on nuclear parameters in the divertor cassette will be minimal.

The neutronics calculations have been performed using the continuos energy MCNP-4A code with cross section data from FENDL-1 to determine the detailed spatial distribution of the nuclear parameters in the divertor cassette. The nuclear parameters were provided at the 103 cassette regions used in the model. These parameters included power density, atomic displacement and helium production. The largest heating and damage occurs in the dome PFC which has full view of the plasma. The power density in the W PFC at the dome is 16.4 W/cm^3. The total nuclear heating in the 60 divertor cassettes is 101.6 MW with the major contributors being the dome, vertical targets, and wings. The peak helium production in the VV behind the pumping ducts is 0.2 He appm/FPY implying that rewelding might be feasible. In addition, helium production in the divertor port wall is less than 0.04 He appm/FPY.

REFERENCES

[1] Technical Basis for the ITER Detailed Design Report, Cost Review and Safety Analysis, ITER EDA Documentation Series, International Atomic Energy Agency, Vienna, December 1996.

[2] Technical Basis for the ITER Interim Design Report, Cost Review and Safety Analysis, ITER EDA Documentation Series, No. 7, International Atomic Energy Agency, Vienna, April 1996.

[3] M. Sawan, L. Petrizzi, R. Santoro, and D. Valenza, "Three-Dimensional Neutronics and Shielding Analyses for the ITER Divertor," Fusion Technology, 30, 601 (1996).

[4] J. Briesmeister, Ed., "MCNP, A General Monte Carlo N-Particle Transport Code, Version 4A," LA-12625-M, (1993).

[5] R. MacFarlane, "FENDL/MC-1.0, Library of Continuous Energy Cross Sections in ACE Format for MCNP-4A," Summary Documentation by A. Pashchenko, H. Wienke and S. Ganesan, Report IAEA-NDS-169, Rev. 3, International Atomic Energy Agency (Nov. 1995).